

Incorporation of Sb in ZnO Nanostructures Through Hydrothermal Process

A. Escobedo Morales¹, U. Pal^{1,*}, and M. Herrera Zaldivar²

¹Instituto de Física, Benemérita Universidad Autónoma de Puebla, Apdo. Postal J-48, C.P. 72570, Puebla, Pue., Mexico

²Centro de Ciencias de la Materia Condensada, Universidad Nacional Autónoma de México, Apdo. Postal 2681, C.P. 22800, Ensenada, Baja California, Mexico

Incorporation of dopants in optoelectronic semiconductor nanostructures has been a matter of great interest in recent times. While such doping has been performed almost routinely using physical methods, use of low-cost chemical techniques for that purpose is still rare. We incorporated antimony in zinc oxide (ZnO) nanostructures through a low temperature hydrothermal method. In as-grown nanostructures, antimony remains partially in Sb₂O₃ phase. On thermal annealing at 500 °C, it dissociates and antimony incorporates into ZnO mainly by substituting zinc from the crystal lattice. Incorporation of Sb drastically modifies the morphology of the ZnO nanostructures. While incorporation of Sb in low concentration promotes the formation of uniform prismatic ZnO nanorods probably due to catalytic effect, high concentration of Sb causes the formation of rounded shaped nanoparticles due to high interfacial compressive stress. Incorporated Sb in the ZnO nanostructures remains inhomogeneously distributed. The optical band gap of the ZnO nanostructures increases a bit for lightly doped samples but it decreases for heavy doping.

Keywords: Zinc Oxide, Antimony Doping, Hydrothermal Synthesis.

1. INTRODUCTION

ZnO is one of the most promising materials to develop the next generation of electronic and optoelectronics devices. Since ZnO has a wide direct band (3.37 eV at room temperature) and a large exciton binding energy (60 meV)¹ it is a potential candidate for the fabrication of blue emitting diodes and UV lasers.^{2,3} In recent years, considerable efforts to obtain ZnO nanostructures have been carried out since the density of states near the band gap edges is enhanced in such structures, which results in lower threshold for lasing (≈ 200 kW/cm²)⁴ than its bulk counterpart (≈ 300 kW/cm²).⁵ Shallow states can be introduced in the band gap on doping these nanostructures. It is believed that such extrinsic defects might reduce the lasing threshold even further. Therefore, great attempts to obtain doped ZnO nanostructures incorporating elements of groups III, IV and V like Al, Ga, In, Sn, N and Sb^{6–9} have been made. Physical methods like metal organic chemical vapor deposition (MOCVD),¹⁰ thermal evaporation^{7,11,12} and pulsed laser deposition¹³ are common routes to obtain doped nanostructures. Nevertheless, reports using low cost chemical synthesis are still rare.^{14–16} The principal challenges

to obtain doped metal oxides nanostructures by chemical synthesis methods are the solubility of precursor salts in the reaction solution, homogeneous distribution of doping atoms in the host lattice, and formation of a second phase due to segregation of doping element.

Here we report the synthesis of antimony doped zinc oxide nanostructures through a low temperature hydrothermal process. Effects of antimony doping on the crystallinity and morphology of the nanostructures are studied by X-ray diffraction (XRD) and scanning electron microscopy (SEM). Incorporation and distribution of dopant in the nanostructures are studied by energy dispersive spectroscopy (EDS) and elemental mapping. Possible mechanism of Sb incorporation in ZnO nanostructures is discussed.

2. EXPERIMENTAL DETAILS

Ethylenediamine (NH₂(CH₂)₂NH₂, EDA; Baker, 99.9%), zinc acetate dihydrate (Zn(CH₃COO)₂ · 2H₂O; Aldrich, 99.99%), sodium hydroxide (NaOH; Aldrich, 99.99%), and antimony acetate (Sb(CH₃COO)₂; Aldrich, 99.99%) were purchased commercially and used as received without further purification. In a round bottom three-neck flask an alkaline aqueous solution was prepared mixing 108 ml

*Author to whom correspondence should be addressed.

of ultra pure deionized water (E-pure Barnstead system, 18.0 M Ω cm) and 12 ml of EDA under vigorous stirring. To the previous solution, 10.25 g of zinc acetate was added. Then 1.70 g of anhydrous NaOH was added to the mixture solution under agitation. The final pH of the reaction mixture was about 12.15. The hydrothermal reaction was carried out at 110 °C for 15 h introducing the reaction flask in an oil bath to homogenize the temperature in the solution. Formation of some white material at the inner wall and at the bottom of the reaction flask was observed. Once the reaction solution is cooled down to room temperature, the solid product was extracted by decantation, washed by deionized water several times and dried in a muffle furnace keeping the temperature below 100 °C for 2 h. To obtain the doped samples, once the zinc acetate was dissolved, 0.0698, 0.1388 or 0.2793 g of antimony acetate was added to the EDA-water solution to prepare nominal 0.5%, 1.0% and 2.0% antimony doped zinc oxide samples, respectively. The final pH of the reaction mixture decreased a bit (\sim 12.1) on addition of antimony acetate. After the hydrothermal synthesis, the four samples were annealed at 500 °C for 2 h under nitrogen flow in a horizontal furnace.

The nanostructures were characterized by X-ray diffraction (XRD, Phillips X'Pert diffractometer with Cu K α radiation), scanning electron microscopy (SEM, Jeol JSM 5300), energy dispersive spectroscopy (EDS, Thermo Noran SuperDry II), and diffuse reflectance spectroscopy (DRS, Varian Cary 100 UV-Vis Spectrophotometer with DRA-CA-30I diffuse reflectance accessory).

3. RESULTS AND DISCUSSION

Figure 1 shows the typical SEM micrographs of the as-grown ZnO nanostructures with different nominal concentrations of antimony. In the undoped sample, formation of needle shaped rods of 100–650 nm diameters and of about 4.5 μ m average length is clear. The SEM micrographs (Fig. 1) revealed a drastic morphology change of the nanostructures on Sb incorporation. More the concentration of Sb, more was the change in morphology. With the increase of Sb concentration, the needle shaped structures first changed to perfect prismatic rods, mostly of uniform diameter (Fig. 1(b)), and then formed particles along with nanorods (Fig. 1(c)). For the 2% (nominal) of Sb doping, only particles were formed (Fig. 1(d)) without any 1D structure.

XRD patterns of the as-grown samples are shown in Figure 2(a). The spectrum of the undoped sample revealed sharp diffraction peaks indicating good crystallinity. All the diffraction peak positions match with the standard diffraction pattern of wurtzite ZnO lattice (JCPDS 36-1451). However, on Sb doping the intensity of the peaks reduced gradually indicating a reduction of crystallinity. Moreover, for the highest concentration of Sb (nominal 2 at%), beside the diffraction peaks related to ZnO, there appeared several low intensity peaks which correspond to orthorhombic (JCPDS 71-0383) and cubic (JCPDS 72-1334) phases of Sb₂O₃ (Fig. 3). So the Sb incorporated at high concentration in ZnO remained partially phase separated. It must be mentioned that no peak

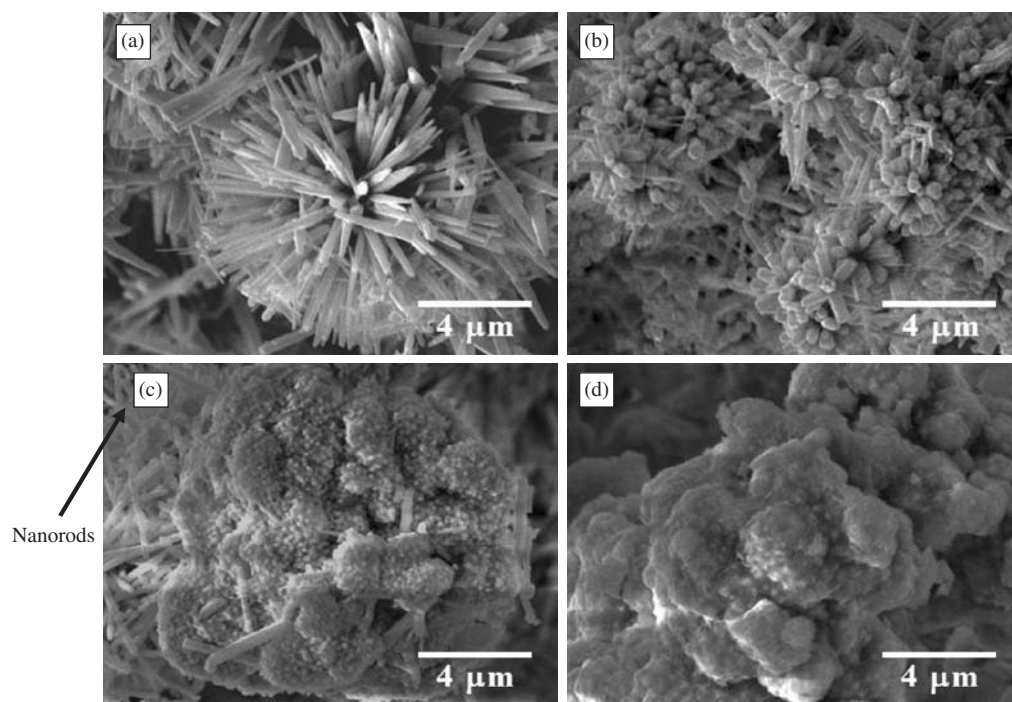


Fig. 1. Typical SEM micrographs of as-grown (a) undoped, (b) 0.5% antimony doped, (c) 1.0% antimony doped, and (d) 2.0% antimony doped ZnO samples.

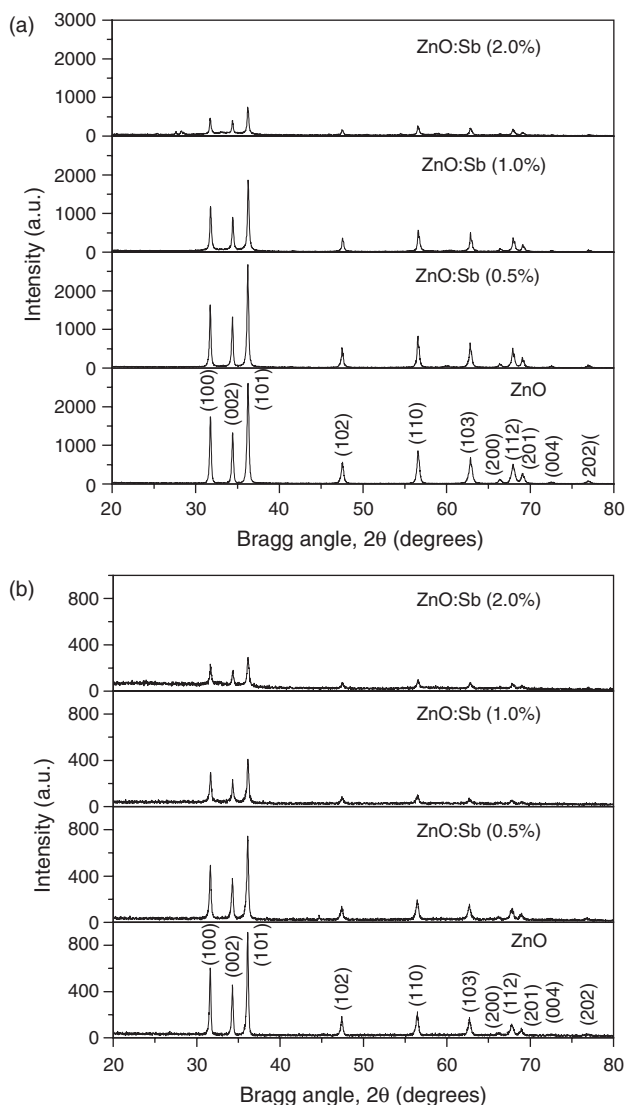


Fig. 2. XRD patterns of ZnO nanostructures: (a) as-grown, and (b) after thermal annealing at 500 °C.

related to elemental Sb was detected in the XRD patterns of the doped samples. To eliminate the oxide phase of antimony in the doped samples and promote the diffusion of Sb into ZnO lattice, all the samples were annealed at 500 °C for 2 h under nitrogen flow. The annealing temperature of the nanostructures (500 °C) was chosen to be lower than the melting temperature of Sb_2O_3 (560 °C and 656 °C for cubic and orthorhombic, respectively).¹⁷ In Figure 2(b), the XRD patterns of the annealed samples are shown. Absence of any diffraction peak related to the oxide phase of antimony in the annealed samples indicates its dissociation on thermal annealing.

The morphology of the annealed samples were studied further and presented in Figure 4. While the morphology of the undoped and 0.5% Sb doped samples did not show any drastic variation on thermal annealing, for the nanostructures with 1% and 2% Sb doping it changed

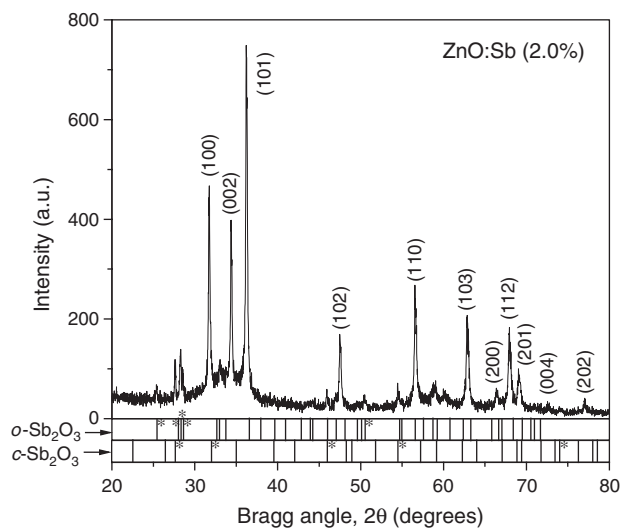


Fig. 3. XRD pattern of as-grown ZnO:Sb (2%) in amplified intensity scale. Apart from the peaks related to ZnO, several low intensity peaks related to cubic and orthorhombic Sb_2O_3 with low intensity can be noticed. The diffraction peaks having high intensities (according to JCPDS data) are marked.

remarkably. On thermal annealing, the mixed rod and particle like structures of as-grown 1% Sb doped sample changed to purely rod like (Fig. 4(c)). Prismatic nanorods of very uniform diameter (ca. 350 nm) were formed. On the other hand, the 2% Sb doped ZnO sample revealed agglomerates of rounded shaped particles (diameter ca. 750 nm) with some wool like spines over them. Therefore, while the Sb doping concentration affects the morphology of the ZnO nanostructures, the annealing process also affects it significantly.

Though the exact mechanism of morphology change in ZnO nanostructures on Sb doping is not yet clear, the change might be a stress-driven effect. Due to the sizeable mismatch of linear expansion coefficient between zinc oxide and Sb (Sb_2O_3), ($\alpha_{\text{ZnO}}(800 \text{ K}) = 6.32 \times 10^{-6} \text{ K}^{-1}$ and $\alpha_{\text{Sb}}(800 \text{ K}) = 11.8 \times 10^{-6} \text{ K}^{-1}$)^{18,19} a large compressive stress might have developed at the interface of the two materials. As the strain energy is much larger than the surface energy, it modifies the morphology of the ZnO surface at a given temperature, as a driving force for the formation of patterned structures. Similar stress driven mechanism has been assigned to the formation of Fibonacci number patterns in Ag core/ SiO_x shell structures by Li et al.²⁰

On the other hand, the incorporated Sb in our synthesis process might have acted as catalyst for the oriented growth of uniform prismatic ZnO nanorods, as in the case of 1% Sb doped sample. Recently Liang et al.²¹ have shown that incorporation of Ga in the vapor phase growth of ZnO nanostructures can catalyze the growth process and controls the morphology of the nanostructures considerably. The incorporated Ga favors the growth of ZnO nanostructures along [0001] direction maintaining the ZnO layers well oriented.

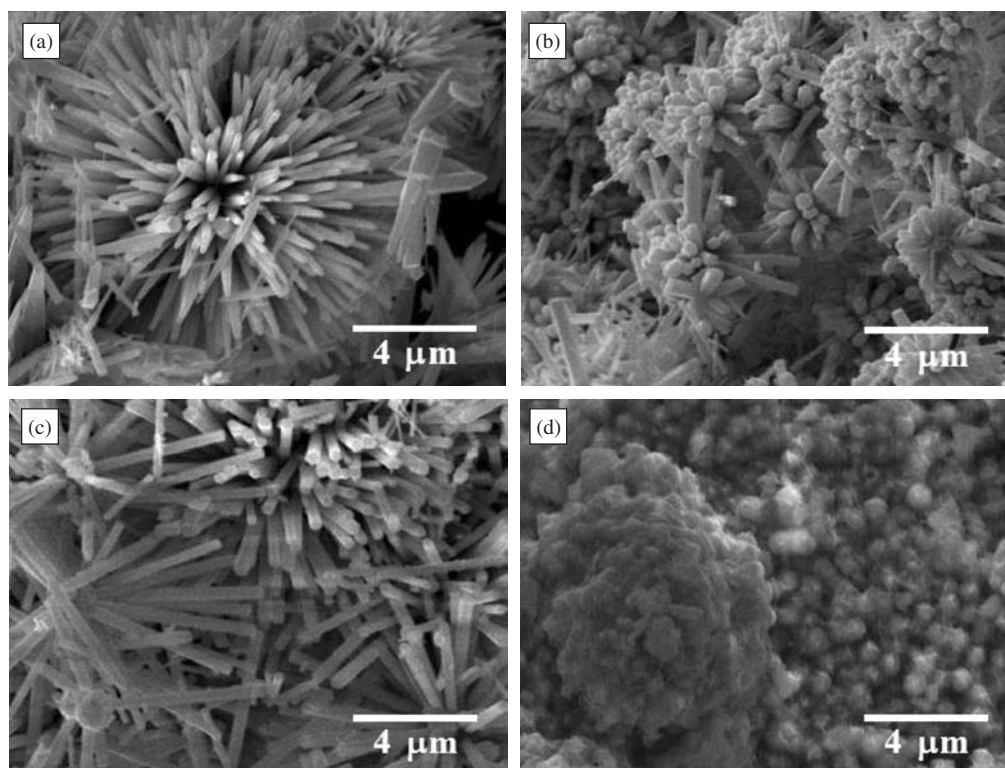


Fig. 4. Typical SEM micrographs of annealed samples; (a) undoped, (b) 0.5% antimony doped, (c) 1.0% antimony doped and (d) 2% antimony doped ZnO samples.

We believe, in our Sb doped ZnO nanostructures, while for the samples with low Sb concentrations (0.5% and 1%, nominal) the second mechanism might be responsible for the well oriented and uniform growth of prismatic ZnO nanorods, for high concentration of Sb (nominal 2 at%) the former mechanism is in vogue. When Sb is incorporated in high concentration, the effect of interfacial compressive stress is high, especially when the samples were cooled to room temperature after thermal annealing. Formation of particle like morphology in our 2% Sb doped sample after thermal annealing justifies well the action of compressive stress in them.

The change of crystallinity of the nanostructures due to Sb doping could be monitored from the analysis of their main XRD peaks. In Table I, the position and the full width at half maximum (FWHM) of (100) and (002) peaks of the annealed samples are presented. As can be noticed, while the peak positions of the doped samples shifted towards

higher Bragg angle with the increase of doping concentration, their FWHM increased simultaneously. While the increase of FWHM in the doped samples indicates a reduction of crystallinity, the shift of peak positions indicates the shrinkage of their lattice constants (both a and c). Such a reduction of lattice constant values might be due to the compressive stress developed at the interface of Sb and ZnO during the segregation process as described earlier.

The elemental composition of the nanostructures was analyzed by EDS. There appeared no emission peak other than Zn, O and Sb in the samples, indicating the absence of any other impurity in them. In Table II, the elemental compositions of the annealed doped and undoped samples are presented. It must be mentioned that due to inhomogeneous distribution of the dopant, the composition of the samples varied from place to place. Therefore, the EDS analysis for each sample was performed at different places and the final composition was estimated by taking their average.

Table I. Position and FWHM of the main diffraction peaks of the annealed ZnO:Sb samples.

| Nominal antimony concentration(at%) | (100) diffraction peak position and its FWHM (degrees) | (002) diffraction peak position and its FWHM (degrees) |
|-------------------------------------|--|--|
| 0.0 | 31.62 (0.23) | 34.28 (0.25) |
| 0.5 | 31.64 (0.27) | 34.28 (0.29) |
| 1.0 | 31.67 (0.30) | 34.32 (0.29) |
| 2.0 | 31.67 (0.39) | 34.34 (0.40) |

Table II. EDS composition analysis of the doped and undoped ZnO nanostructures after annealing.

| Nominal antimony concentration (at%) | Zn: O:Sb (at%) (EDS average) |
|--------------------------------------|------------------------------|
| 0.0 | 50.00:50.00:0.00 |
| 0.5 | 49.68:50.14:0.18 |
| 1.0 | 49.03:50.42:0.55 |
| 2.0 | 46.20:51.90:1.90 |

To study the distribution of Sb in the nanostructures, we performed elemental mapping in a doped sample. In Figure 5, elemental mappings for all three elements (Zn, O and Sb) in the 2% Sb doped ZnO are shown. From the figure we can observe that while the distribution of zinc in the sample was homogeneous, oxygen and antimony remained inhomogeneously distributed. However, to some extent, the distributions of Sb and O were similar. From the composition presented in Table II, we can see that the incorporated Sb in the samples was less than their nominal concentrations. With the increase of Sb concentration, while the concentration of O in the samples remained almost fixed, the concentration of zinc decreased significantly. We believe the incorporated Sb atoms substitute Zn atoms from their lattice sites in ZnO nanostructures.

Group V elements such as N,²² P,²³ and As²⁴ have been tried experimentally as *p*-type dopants in ZnO. Among them, nitrogen was seen to be the most suitable dopant due to its similar atomic radius (0.75 Å) to that of oxygen (0.73 Å). Possibility of *p*-type doping with larger radius group V atoms such as phosphorous and arsenic has also been explored using first-principles calculations by Limpitjumnong et al.²⁵ It is generally considered that a group V element atom must substitute the oxygen atom to generate holes in ZnO. However, it was suggested²⁵ that the *p*-type conductivity in size-mismatched impurity doped ZnO is derived through the formation of defect complex like $X_{Zn} - 2V_{Zn}$, where X denotes a group V atom other than N. The group V atom substitutes on the Zn site,

forming a donor, and then inducing two Zn-vacancy acceptors. Very recently Kang et al.²⁶ have demonstrated the formation of such two Zn-vacancy acceptors in arsenic doped ZnO thin films through photoluminescence and X-ray photoelectron spectroscopic studies.

In our Sb doped ZnO nanostructures, we believe that due to large mismatch of atomic radius between Sb and O (the atomic radius of Sb and O are 1.38 Å and 0.73 Å, respectively), incorporated Sb atoms substituted Zn atoms of similar atomic radius (1.31 Å), rather than oxygen. A clear decrease of Zn content in the doped samples (Table II) justifies our assumption. However, a further investigation is in progress to support our assumption experimentally.

To study the effect of antimony doping on the optical bandgap energy (E_g) of our ZnO nanostructures, diffuse reflectance spectra were measured on them. It is well known that the bandgap of semiconductors can be tuned by reducing their size to the nanometer scale. A blue shift of optical bandgap occurs due to the quantum confinement of charge carriers. The effect can be detected for ZnO nanoparticles less than 7 nm.²⁷ On the other hand, by doping a semiconductor with appropriate elements, both blue and red shifts can be observed.²⁸ As the diameter of our nanostructures was big enough, the occurrence of quantum confinement effect is not expected in them. Hence, the observed change in bandgap energy in them can be attributed solely to the antimony doping. In Figure 6, the diffuse reflectance spectra of the samples are presented.

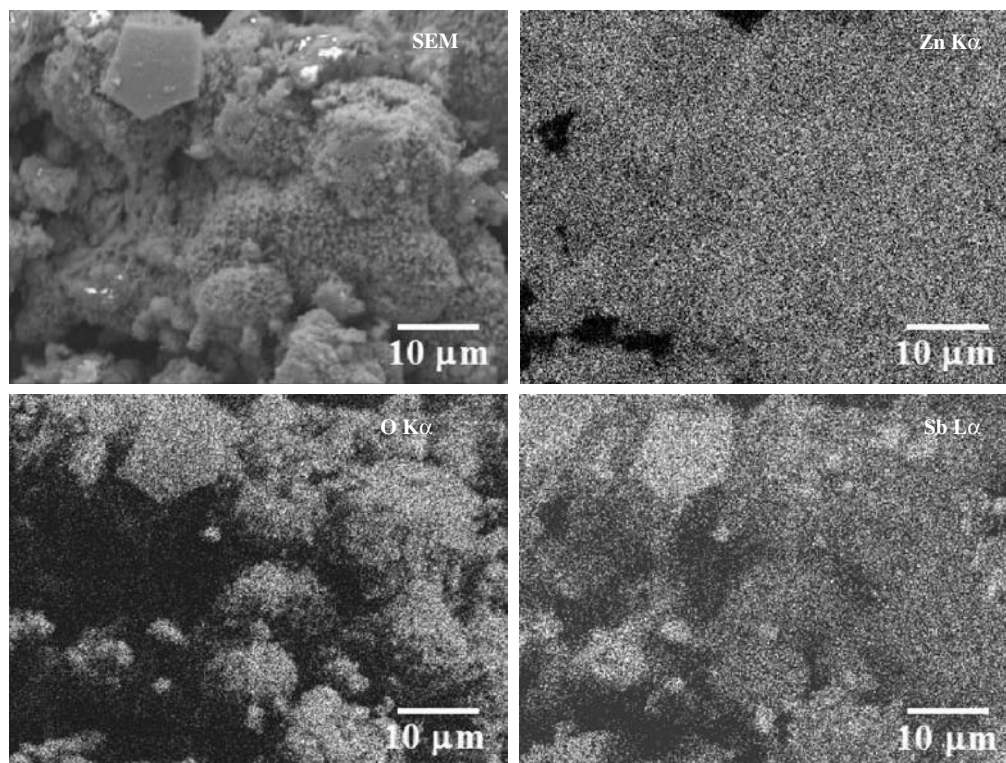


Fig. 5. EDS elemental mappings for the annealed ZnO:Sb (2%) sample.

The decrease of reflectance onset on increasing Sb concentration in the nanostructures is due to deterioration of their crystal quality. However, the effect is more pronounced in the annealed samples.

A detailed study of the band gap energy evolution in our Sb doped ZnO nanostructures can be obtained by applying Kubelka-Munk²⁹ treatment to the diffuse reflectance spectra (Fig. 6). Once the so-called remission or Kubelka-Munk function $[F(R_\infty)]$ is calculated from reflectance measurements, it is possible to know the E_g of the powder samples. The details of the Kubelka-Munk treatment and band gap evaluation procedures are discussed elsewhere.³⁰ Figure 7 shows the Kubelka-Munk plots used to estimate the E_g values for the samples. We can see that the bandgap shifts slightly towards higher energy on Sb incorporation in the as-grown nanostructures. After annealing, the bandgap did not change noticeably (Fig. 7(b)) for lower doping concentrations. However, it shifted about 0.03 eV towards lower energy for 2% Sb doping. Wang et al.²⁸ have reported a decrease in E_g around 0.06 eV in 2% Cd doped ZnO nanocrystals. Gulino and Fragala³¹ have

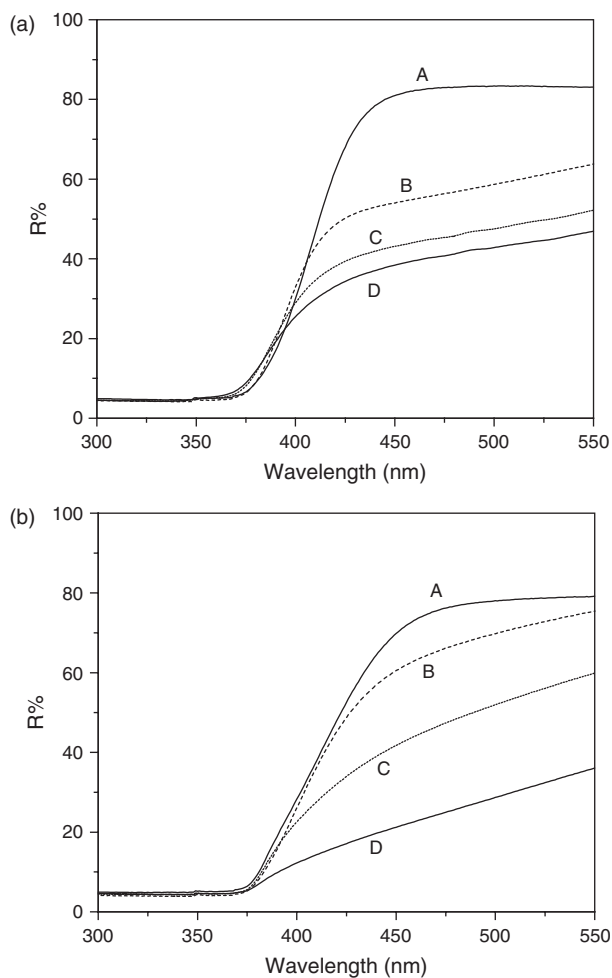


Fig. 6. Diffuse reflectance spectra of the (a) as-grown, and (b) thermally treated ZnO nanostructures. A, B, C and D labels correspond to un-doped, 0.5%, 1.0%, and 2.0% antimony doped samples respectively.

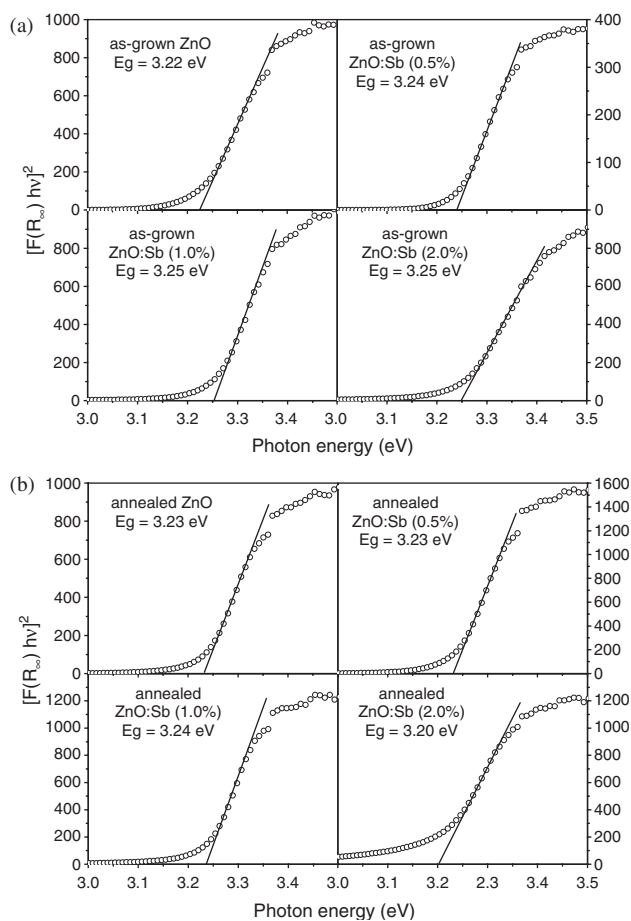


Fig. 7. Band gap energy estimation for (a) as-grown, and (b) annealed samples using Kubelka-Munk treatment.

observed a similar reduction of optical bandgap in 1.8% Sb-doped ZnO thin films.

While a small increase of band gap in our as-grown Sb-doped nanostructures might be due to the formation of Sb_2O_3 phase in them (bandgap of Sb_2O_3 in cubic phase ≈ 3.62 eV and of orthorhombic phase ≈ 3.30 eV)³² the decrease of bandgap energy in 2% Sb doped nanostructures after thermal annealing in inert ambient indicates the incorporation of elemental Sb in ZnO.

We believe that after thermal annealing, in low doped samples, Sb atoms incorporate at the interstitial lattice sites of ZnO, compensating its n -type conductivity to some extent, and for heavy doping, Sb atoms substitute Zn atoms from their lattice sites transforming the nanostructures to p -type. However, electrical measurements on the samples are needed to be performed further to confirm this assumption.

4. CONCLUSIONS

ZnO nanostructures could be doped successfully with group V element Sb through a low temperature hydrothermal process and subsequent thermal annealing in inert

atmosphere. The morphology and crystallinity of ZnO nanostructures change drastically on incorporation of Sb. While a low Sb doping has a catalytic effect on directional growth of uniform ZnO nanostructures, for heavy Sb doping, high interfacial compressive stress between Sb and ZnO changes their morphology drastically. Incorporated Sb in the nanostructures probably substitute Zn atoms from their lattice sites, and remain inhomogeneously distributed. Optical bandgap of ZnO nanostructures does not vary significantly for low Sb doping. However, for high Sb doping it decreases.

Acknowledgments: We are thankful to E. Aparicio Ceja for her help in taking XRD traces of the nanostructures. The work is partially supported by CONACyT, Mexico (Grant No. 46269) and UC-MEXUS-CONACyT (Grant No. CN-05-215).

References and Notes

1. C. Klingshirn, *Phys. Stat. Sol. B* 71, 547 (1975).
2. Z. K. Tang, G. K. L. Wong, P. Yu, M. Kawasaki, A. Ohtomo, H. Koinuma, and Y. Segawa, *Appl. Phys. Lett.* 72, 3270 (1998).
3. M. H. Huang, S. Mao, H. Feick, H. Yan, Y. Wu, H. Kind, E. Weber, R. Russo, and P. Yang, *Science* 292, 1897 (2001).
4. J. C. Johnson, H. Yan, R. D. Schaller, L. H. Haber, R. J. Saykally, and P. Yang, *J. Phys. Chem. B* 105, 11387 (2001).
5. H. Cao, Y. Y. Xu, D. Z. Zhang, S. H. Chang, S. T. Ho, E. W. Seelig, X. Liu, and R. P. H. Chang, *Phys. Rev. Lett.* 84, 5584 (2000).
6. C. L. Hsu, S. J. Chang, H. C. Hung, Y. R. Lin, C. J. Huang, Y. K. Tseng, and I. C. Chen, *J. Electrochem. Soc.* 152, G378 (2005).
7. S. Y. Bae, C. W. Na, J. H. Kang, and J. Park, *J. Phys. Chem. B* 109, 2526 (2005).
8. B. Wang, M. J. Callahan, L. O. Bouthillette, C. Xu, and M. J. Suncavage, *J. Cryst. Growth* 287, 381 (2006).
9. D. W. Zeng, C. S. Xie, B. L. Zhu, R. Jiang, X. Chen, W. L. Song, J. B. Wang, and J. Shi, *J. Cryst. Growth* 266, 511 (2004).
10. J. Zhong, S. Muthukumar, Y. Chen, Y. Lu, H. M. Ng, W. Jiang, and E. L. Garfunel, *Appl. Phys. Lett.* 83, 3401 (2003).
11. C. Xu, M. Kim, J. Chun, and D. Kim, *Appl. Phys. Lett.* 86, 133107 (2005).
12. J. Jie, G. Wang, X. Han, Q. Yu, Y. Liao, G. Li, and J. G. Hou, *Chem. Phys. Lett.* 387, 466 (2004).
13. M. Yan, H. T. Zhang, E. J. Widjaja, and R. P. H. Chang, *J. Appl. Phys.* 94, 5240 (2003).
14. A. Escobedo, M. Herrera, and U. Pal, *Opt. Mater.* 29, 100 (2006).
15. S. B. Majumder, M. Jain, P. S. Dobal, and R. S. Katiyar, *Mater. Sci. Eng. B* 103, 16 (2003).
16. T. Agne, Z. Guan, X. M. Li, H. Wolf, T. Wichert, H. Natter, and R. Hempelmann, *Appl. Phys. Lett.* 83, 1204 (2003).
17. E. B. Gel'man, Handbook of Physical Quantities, edited by I. S. Grigoriev, E. Z. Meilikhov, and A. A. Radzing, CRC Press, USA (1997) Chap. 12, p. 370.
18. A. A. Khan, *Acta Cryst. A* 24, 403 (1968).
19. E. B. Gel'man, Handbook of Physical Quantities, edited by I. S. Grigoriev, E. Z. Meilikhov, and A. A. Radzing, CRC Press, USA (1997) Chap. 10, p. 288.
20. C. Li, X. Zhang, and Z. Cao, *Science* 309, 909 (2005).
21. Y. Liang, X. Zhang, L. Qin, E. Zhang, H. Gao, and Z. Zhang, *J. Phys. Chem. B* 110, 21593 (2006).
22. D. C. Look, J. W. Hemsky, C. W. Litton, R. L. Jones, D. B. Eason, and G. Cantwell, *Appl. Phys. Lett.* 81, 1830 (2002).
23. K. K. Kim, H. S. Kim, D. K. Hwang, J. H. Lim, and S. J. Park, *Appl. Phys. Lett.* 83, 63 (2003).
24. Y. R. Ryu, S. Zhu, D. C. Look, J. M. Wrobel, H. M. Jeong, and H. W. White, *J. Cryst. Growth* 216, 330 (2000).
25. S. Limpijumnong, S. B. Zhang, S.-H. Wei, and C. H. Park, *Phys. Rev. Lett.* 92, 155504 (2004).
26. H. S. Kang, G. H. Kim, D. L. Kim, H. W. Chang, B. D. Ahn, and S. Y. Lee, *Appl. Phys. Lett.* 89, 181103 (2006).
27. E. A. Muelenkamp, *J. Phys. Chem. B* 102, 5566 (1998).
28. Y. S. Wang, P. J. Thomas, and P. O'Brien, *J. Phys. Chem. B* 110, 21412 (2006).
29. P. Kubelka and F. Munk, *Z. Tech. Phys.* 12, 593 (1931).
30. A. Escobedo, E. Sánchez, and U. Pal, *Rev. Mex. Fis.*, to be published.
31. A. Gulino and I. Fragala, *Chem. Mater.* 14, 116 (2002).
32. N. Tigau, V. Ciupina, G. Prodan, G. I. Rusu, and E. Vasile, *J. Cryst. Growth* 269, 392 (2004).

Received: 5 December 2006. Accepted: 24 May 2007.